Periodica Polytechnica
Mechanical Engineering

# Optimum Finger Spacing for Swimmers

60(1), pp. 1-14, 2016
DOI: 10.3311/PPme.7721


Bence Dániel Darázs[1*], György Paál[1]

RESEARCH ARTICLE

Received 22 September 2014; accepted after revision 04 November 2015

***Abstract***

*The purpose of this study was to investigate the effect of spreading the fingers in human swimming. Two-dimensional CFD simulations were carried out to gain insight into this problem, modelling the fingers by equidistant cylinders. One, two and then four cylinders were studied with varying distance. The effect of the thumb was neglected. The drag coefficients of the individual cylinders in the assembly were then compared with each other and other previously published data. The power spectrum of the drag coefficients and videos of the velocity contours were also examined. The dominant frequency, its subharmonics as well as the qualitative appearance of the flow varied strongly with the finger distance. Contrary to other studies and our expectations, the optimum finger spacing proved to be the zero distance configuration.*

***Keywords***

*CFD, Swimmer, Finger spacing, Cylinder*

[1] Departement of Hydrodynamic Systems, Faculty of Mechanical Engineering, Budapest University of Technology and Economics, 1111 Budapest, Műegyetem rkp. 3., Hungary

[*] Corresponding author, e-mail: darazs.bence@gmail.com

## 1 Introduction

The optimum finger spacing in human swimming is an interesting and controversial problem. Most of the studies treating this question concluded that an optimum spacing does exist, so that a swimmer is able to produce a greater force if he does not close his fingers entirely but spreads them slightly, based upon two- or three-dimensional (2D, 3D) CFD simulations.

Marinho et al. [1] applied a 3D model of a human hand in the computational domain, and investigated the effect of spreading the fingers on the drag and lift coefficients of the hand. Minetti et al. [2] used a similar hand model, though the position of the thumb was the same while the finger spread varied. Both of these studies concluded that an optimum finger spacing in human swimming exists. Bilinauskaite et al. [3] also ran several 3D simulations with a model of a human hand, focusing on not just the finger spacing but the position of the arm during a swimming stroke. He concluded that the optimum finger spacing depends on the actual stroke phase. The results also showed that the drag coefficient has a maximum when the fingers are closed together, have no gap between them and the arm is exactly below the shoulder. Lorente et al. [4] carried out 2D simulations to determine the optimum spacing between the fingers. The fingers were modeled as cylinders, the effect of the thumb was disregarded. This study also found that the drag coefficient of the cylinders had a maximum when there is a little gap between them.

The studies do not agree on the optimum size of the gap between the fingers. Also many authors do not mention any details about several decisive parameters of the simulations such as the size and resolution of the numerical grid, the timestep and the turbulence model.

Simplified, 2D models, consisting of equidistant circular cylinders represent a lower level of modelling, yet they allow a much more precise and systematic study of the effect of finger spacing. Building on the new and solid knowledge obtained from these models, 3D, more realistic models can be studied on a firm basis.

Sumner et al. [5] examined two-cylinder arrangements with different gap sizes between the cylinders. According to their results, between $T/D = 2.2$ and 1.2 the vortex shedding behind the cylinders was very distinctive compared to other $T/D$

ranges and a larger wake was formed consistently behind one cylinder (for the definition of $T/D$ see Fig. 1). Wang and Zhou [6] also carried out measurements focusing on the vortex shedding pattern behind two cylinders. They concluded that the previously mentioned regime with a distinctive flow pattern does exist, and at $Re = 5900$ it was between $T/D = 2$ and 1.2.

The details - such as the Reynolds number - of the previously mentioned studies are shown in Table 1.

**Table 1** Details of the cited studies

| | *Re* [-] | Other details |
|---|---|---|
| This study | 33610 | 2D model with cylinders, transient simulation |
| [1] | 29940 | 3D hand model, steady-state simulation |
| [2] | - | 3D, steady-state simulation |
| [3] | - | 3D hand model, steady-state simulation, v = 1.79 − 2.75 [m/s] |
| [4] | 20-100 | 2D model with cylinders, steady-state simulation |
| [5] | 500-3000 | Measurement with cylinders |
| [6] | 120-1100; 5900 | Measurement with cylinders |
| [7] | 26000, 40000, 50000 | Measurement with cylinders |
| [9] | $1.5\cdot10^4$ ..$4.5\cdot10^4$ | Measurement with cylinders |
| [10] | $10^5$ ..$10^7$ | 3D model with a cylinder |
| [11] | $10^5$ ..$10^7$ | 3D model with a cylinder |

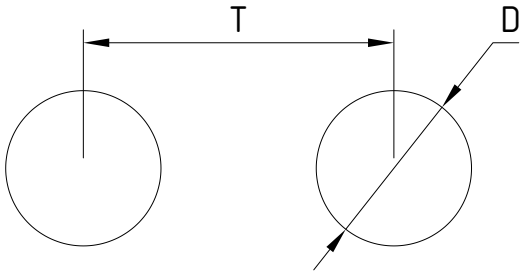


**Fig. 1** The definiton of $T$ and $D$ .

Our goal with this study was to thoroughly and systematically examine the drag coefficient of two and four equidistant cylinders with different spacings between them and to find the maximum $C_D$. The swimmer's fingers were modelled as cylinders, the effect of the thumb was not considered and the numerical model was two-dimensional. The structured mesh was created using ICEM CFD and the solver was ANSYS CFX.

At the beginning only one cylinder was examined. The results of the simulations were then compared to other CFD simulations and mesurements. This was necessary in order to find a proper grid, turbulence model and timestep for the two and four cylinder arrangements.

After this, two and then four cylinders were placed in the domain. The spacing between the cylinders was equidistant. The drag coefficient of the cylinders were recorded from $T/D =$ 13 to $T/D = 1$ (for notations see Fig. 1). Finally, the power spectra of the drag coefficients were presented and analysed.

## 2 Computational setup based on the flow around a single cylinder

First, only one cylinder was analysed in a crossflow to find the proper numerical grid and the turbulence model. The shape of computational domain and the boundary conditions are shown in Fig. 2. Several meshes were examined with different numbers of elements, domain sizes and wall-bounding first cell heights. The time step was chosen according to the Strouhal number associated with the vortex shedding frequency. Two similar turbulence models, the SST (**`Shear Stress Transport`**) and the Scale Adaptive SST (**`SAS SST`**) were tested.

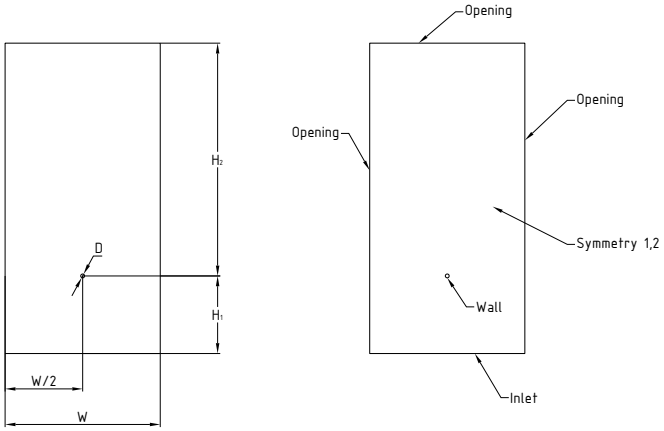


**Fig. 2** The shape of the computational domain and the applied boundary conditions.

A constant, $v_\infty = 2\ m/s$ velocity was defined on the **`Inlet`** boundary condition, while a constant 0 relative pressure was set on the other three sides of the rectangle, called **`Opening`** boundary condition. **`Opening`** allows flow in both directions through the surface. The applied **`Wall`** boundary condition on the cylinder surface was a no-slip wall and the 2D nature of the flow was ensured by the symmetry boundaries (**`Symmetry 1,2`**), on the top and bottom surfaces. The height of the computational domain was 1 cell.

Several measurements and CFD simulations were carried out in the past regarding the drag coefficient of a cylinder in crossflow. Bruschi et al. [7] compared three different methods for measuring the pressure distribution around a cylinder. He also calculated the drag coefficient of the cylinder for three Reynolds numbers (26000, 40000, 50000). Tritton [8] published a figure which shows the drag coefficient of a cylinder versus the Reynolds number from $Re = 10^{-1}$ ..$10^7$. Hover et al. [9] compared the drag coefficients, the Strouhal numbers and the lift coefficients of a cylinder with and without tripping wires from

$Re = 1.5 \cdot 10^4..4.5 \cdot 10^4$. Dynnikova [10] carried out CFD simulations focusing on the decrease of the drag coefficient in the critical regime ($Re \approx 10^5 ..10^7$) and compared her results with other measurements and simulations. Benim et al. [11] used RANS (**Reynolds Average Navier Stokes**) turbulence models to predict the drag coefficient of a cylinder in almost the same Reynolds number range as Dynnikova [10] and compared his results with measurements and simulations carried out in the past. Our $Re$ of 33610 corresponds to realistic values during swimming - 2 *m/s* and 15 *mm* cylinder diameter, representing fingers. The above studies indicate that the drag coefficient of the cylinder in crossflow for $Re$ = 33610 is approximately 1.2, which will be our reference value for the simulations.

The Reynolds number in our case was defined as

$$Re = \frac{v_\infty D}{\nu} \tag{1}$$

In Equation (1) $D$ is the diameter of the cylinder (here: $D$ = 15 *mm* and $\nu$ is the kinematic viscosity of water (in this study: $\nu = 8.926 \cdot 10^{-7}\ m^2/s$ and $v_\infty = 2\ m/s$, yielding $Re \approx 33610$).

The drag coefficient of the cylinder in crossflow is defined as follows:

$$C_D = \frac{F_D}{\frac{\rho}{2} v_\infty^2 A} \tag{2}$$

In Equation (2) $F_D$ is the drag force acting on the cylinder, $\rho$ is the density of water (in this case 997 $kg/m^3$), $v_\infty$ is the far-field velocity and $A = Dh$, where $D$ is the diameter and $h$ is the height of the cylinder.

For multiple cylinders the averaged drag coefficient was determined as

$$C_D = \frac{\sum_{i=1}^{n} C_{Di}}{n} = \frac{F_D}{\frac{\rho}{2} v_\infty^2 A}. \tag{3}$$

In Equation (3) $n$ is the number of the cylinders, $F_D$ is the total drag force on all the cylinders and $A$ is the total surface, i.e $n \cdot D \cdot h$.

The appropriate time step can be determined from the Strouhal number. The Strouhal number is defined as follows:

$$St = \frac{fD}{v_\infty} \tag{4}$$

From Equation (4) the frequency of vortex shedding ($f$) behind the cylinder can be determined if the Strouhal number, the diameter of the cylinder ($D$) and the far-field velocity ($v_\infty$) is known. According to Techet [12] the Strouhal number for a single circular cylinder for the Reynolds number used in this study is about 0.2 and nearly constant in a long range around this value. Three different time steps were compared and evaluated. In the beginning, the time step was chosen to be one seventieth of one vortex shedding period ($1/f$):

$$\Delta t = \frac{1}{70 f} = \frac{D}{70 \cdot St \cdot v_\infty} = \frac{0.015[m]}{70 \cdot 0.2 \cdot 2[m/s]} = 5.36 \cdot 10^{-4}[s] \tag{5}$$

After this, the time step was increased and then decreased. The results of the simulations with the different time steps are summarised in Table 5. Based on Table 5, the original time step was chosen for the further simulations because the drag coefficients were the same with both this and the smaller time step.

**Table 2** The drag coefficient of the cylinder ($C_D$) with different time steps.

| $\Delta t \cdot 10^{-4}$ [s] | $C_D$ |
|---|---|
| 2.5 | 1.335 |
| 5 | 1.335 |
| 10 | 1.322 |

## 2.1 Block structure

Two different block structures were examined in this study, one with a smaller and one with a larger O-grid around the cylinder (see Fig. 3). Both of these structures yielded an easy way to refine the mesh near the wall. There were 120 nodes around the cylinder for both of the block structures, the growth ratio of the element heights was about 1.1 and the boundary layer was rougly 30 cells thick. The drag coefficients of the cylinder were compared for the two grid structures and turbulence models. The results are summarised in Table 3.

**Table 3** The drag coefficient of the cylinder ($C_D$) with different block structures and turbulence models.

| O-grid | Number of elements | Turbulence model | $C_D$ |
|---|---|---|---|
| Small | 52672 | SST | 1.091 |
| | 52672 | SAS SST | 1.353 |
| Large | 51840 | SST | 1.067 |
| | 51840 | SAS SST | 1.332 |

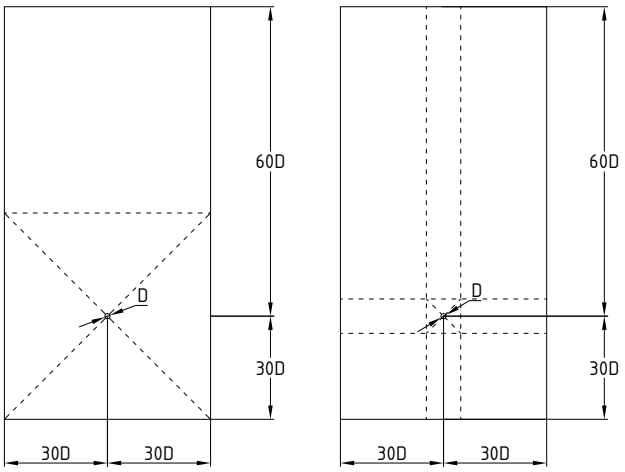


**Fig. 3** The two different block structures used in this study. Left: large O-grid; right: small O-grid

If we take the measurement results ($C_D$ = 1.2) as a basis for comparison, from Table 3 it seems that the mesh with the smaller O-grid is better for the **SST** turbulence model and the mesh with the larger O-grid is more accurate for the **SAS SST** model. Taking these observations into account, three meshes with different numbers of elements were examined in order to optimise the mesh and find a good compromise between accuracy and run-time. Table 4 shows the results of these simulations.

According to Table 4 the mesh with the medium sized elements is sufficient for the **SST** turbulence model and the coarse grid for the **SAS SST** model. Two more meshes were analyzed with the smaller O-grid structure to further reduce the run-time of the simulations. The results are summarised in Table 3.

**Table 4** The drag coefficient of the cylinder ($C_D$) with different mesh sizes.

| O-grid | Mesh | Number of elements | Turbulence model | $C_D$ |
|---|---|---|---|---|
| Small | Coarse | 12287 | SST | 1.047 |
| | Medium | 52672 | | 1.091 |
| | Fine | 214132 | | 1.092 |
| Large | Coarse | 12493 | SAS SST | 1.326 |
| | Medium | 51840 | | 1.332 |
| | Fine | 209625 | | 1.327 |

**Table 5** The drag coefficient of the cylinder ($C_D$) with the **SST** turbulence model and different element numbers.

| O-grid | Number of elements | Turbulence model | $C_D$ |
|---|---|---|---|
| Small | 12287 | SST | 1.047 |
| | 19662 | | 1.083 |
| | 29362 | | 1.097 |
| | 52672 | | 1.091 |
| | 214132 | | 1.092 |

The conclusion from Table 5 is that the mesh with 19 962 elements is still accurate enough regarding the drag coefficient. Two meshes were examined further on: the one with the smaller O-grid and 19962 elements and the other with the larger O-grid and 12 493 elements.

## 2.2 The size of the computational domain

At the beginning $W$ (according to Fig. 2) was reduced. The effect of this reduction on the drag coefficient of the cylinder is summarised in Table 4 for both turbulence models.

Table 6 shows that for the mesh with the smaller O-grid the drag coefficient is quite insensitive to $W$. After examining the streamlines of the flow, $W$ was decided to be 20 $D$ and $H$ to be 60 $D$. Of course the distance behind the cylinder could also be reduced but because of the mesh structure it would only slightly reduce the number of elements.

**Table 6** The drag coefficient of the cylinder ($C_D$) with the SST turbulence model and different domain sizes.

| $H$ / $D$ | O-grid | Turbulence model | $W$ / (2 $D$) | Number of elements | $C_D$ |
|---|---|---|---|---|---|
| 60 | small | SST | 10 | 14042 | 1.071 |
| | | | 15 | 15297 | 1.067 |
| | | | 20 | 16652 | 1.071 |
| | | | 25 | 18107 | 1.077 |
| | | | 30 | 19662 | 1.083 |

**Table 7** The drag coefficient of the cylinder ($C_D$) with the **SAS SST** turbulence model and different domain sizes.

| $H$ / $D$ | O-grid | Turbulence model | $W$ / (2 $D$) | Number of elements | $C_D$ |
|---|---|---|---|---|---|
| 60 | large | SAS SST | 15 | 5250 | 1.195 |
| | | | 20 | 7400 | 1.274 |
| | | | 25 | 9880 | 1.315 |
| | | | 30 | 12493 | 1.326 |

The videos of the velocity contours were also evaluated. Some strange flow phenomena could be observed: a low pressure lane with the width of approximately $D$ was formed, starting at about 5..6$D$ behind the cylinder when the larger O-grid was used. Incase of the smaller O-grid, this distinctive lane was still present but it started only about 10 $D$ behind the cylinder. Based upon these observations, it was decided that the mesh with the smaller O-grid would be applied for the further simulations.

## 2.3 The turbulence model

The choice between the two turbulence models was not obvious. The results of the simulations show that the **SST** model always underestimates the drag coefficient, whereas the **SAS SST** overestimates it. The other problem with these two models was the inconsistency regarding the drag coefficient. The tendency between the resolution of the mesh and the drag coefficient of the cylinder was not unequivocal; neither for the **SST** nor for the **SAS SST** model, although the differences between the medium and fine grids are negligible. The differences between the results of the measurements and the simulations are approximately the same (in the last column of Table 8 the relative error in percentages is shown compared to $C_D$ = 1.2 ) for the two turbulence models.

The grids were also tested with a smaller ($Re$ = 16805) and a larger Reynolds number ($Re$ = 67220) using the **SAS SST** model. The grids remained the same; only the time step was modified according to the Reynolds number to keep the

relative temporal resolution. Even the first cell heights were increased to 0.01 *mm* (ten times of the original 0.001 *mm*) but the results did not show a constant $C_D$, as expected (shown in Table 9 and 10).

**Table 8** The drag coefficient of the cylinder $C_D$ with two different turbulence models.

| O-grid | Number of elements | Turbulence model | $C_D$ | $E_R$ |
|---|---|---|---|---|
| Small | 16652 | SST | 1.071 | 10.75 |
| | | SAS SST | 1.335 | 11.27 |

**Table 9** The drag coefficients of the cylinder ($C_D$) with different Reynolds numbers (first cell height: 0,001 *mm* ).

| O-grid | Number of elements | Turbulence model | *Re* | $C_D$ |
|---|---|---|---|---|
| | | | 16805 | 1.59 |
| Small | 16652 | SAS SST | 33610 | 1.335 |
| | | | 67220 | 1.145 |

**Table 10** The drag coefficients of the cylinder ($C_D$) with different Reynolds numbers (first cell height: 0.01 *mm*).

| O-grid | Number of elements | Turbulence model | *Re* | $C_D$ |
|---|---|---|---|---|
| | | | 16805 | 1.628 |
| Small | 16652 | SAS SST | 33610 | 1.402 |
| | | | 67220 | 1.19 |

The simple SST model was also tested with different first cell heights (i.e. $y^+$ values) and Reynolds numbers. The results are summarised in Table 11.

**Table 11** The drag coefficients of the cylinder with different turbulence models and first cell heights.

| Turbulence model | First cell height [mm] | $y^+$ | $C_D$ |
|---|---|---|---|
| SST | 0.01 | 1.13 | 1.1890 |
| | 0.0088 | 0.984 | 1.1818 |
| | 0.001 | 0.122 | 1.1280 |
| SAS SST | 0.01 | 1.19 | 1.3916 |
| | 0.001 | 0.128 | 1.3356 |

From Table 11 it can be seen that the grid with a $y^+$ value of approximately 1 is very close to our reference value (1.18 and 1.2, respectively). This suggests that the SST turbulence model is more accurate for this problem than its counterpart, the SAS SST.

The choice between the two turbulence models is at this point not obvious, thus we continue using both of them for the two-cylinder arrangements.

## 3 Results for two-cylinder arrangements

After the mesh dependence analysis, the two-cylinder arrangements were investigated. Simulations were run with various $T/D$ ratios from 13 to 1.

The reason we decided to investigate such a wide range of distances is that we were also interested in the question, at what distance the cylinders start to have an effect on each other when they get closer. Of course, it is not likely for a professional swimmer to spread his or her fingers so much that the $T/D$ ratio is over 2 or 3 so from a swimming point a view the most relevant $T/D$ range is between 1 and 2.

All in all, seventeen $T/D$ values were investigated: between $T/D$ = 2..13 seven, between $T/D$ = 1..2, ten different configurations were compared. The width of the computational domain was modified in every case to provide enough space on the side of the cylinders (20 $D$). When $T/D$ was 1.4 or less, the block structure was different around the cylinder from those with larger $T/D$ values (Fig. 6).

### 3.1 Two-cylinder arrangements at a higher Reynolds number

To be able to compare our results with experiments carried out with two finite length cylinders in crossflow [13], a higher Reynolds number (55000) was used in our simulations. This meant a higher free stream velocity (3.27 m/s instead of 2 m/s).The results of the simulations are presented in Table 12 and in Fig. 4.

**Table 12** The averaged drag coefficient of the cylinders at different *T/D* ratios (turbulence model: SST, *Re* = 55000). Here $C_D$ was determined as the sum of the time-averaged drag coefficients of the cylinders.

| T/D [-] | $C_D$ [-] |
|---|---|
| 5 | 1.9467 |
| 3 | 2.1380 |
| 2 | 2.5133 |
| 1.8 | 2.4741 |
| 1.75 | 2.4034 |
| 1.6 | 2.4973 |
| 1.5 | 2.0515 |
| 1.4 | 2.2936 |
| 1.3 | 2.1195 |
| 1.2 | 2.1901 |
| 1.1 | 3.5813 |
| 1 | 2.1866 |

Figure 4 suggests that the SST turbulence model is not adequate for this problem. Although the shape of the curve and the numerical data in the range of $T/D$ = 2..5 is in good agreement with the experimental results, below $T/D$ = 2 an

unexpected oscillation of the drag coefficient appears. All this meant that either the **SST** turbulence model was not sufficient for simulating multiple cylinders or simply the 3 dimensional nature of the flow cannot be captured well enough with only 2 dimensional models.

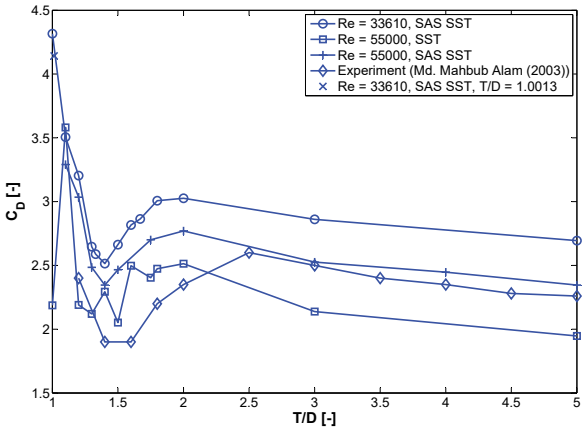


**Fig. 4** Time-averaged drag coefficients versus *T/D*. Here $C_D$ was determined as the sum of the time-averaged drag coefficients of the cylinders.

We investigated both of these possibilities. First, the **SAS SST** turbulence model was used instead of the **SST** in 2D with only one cylinder. The numerical grid was modified in order to keep the value of $y^+$ near 1 and the free stream velocity was set to approximately 3.27 *m*/*s* according to the higher Reynolds number ($Re$ = 55000). The result of this simulation was in good agreement with the experimental data: $C_{D,\,sim}$ = 1.1622 and $C_{D,\,exp}$ = 1.12, respectively. After this,simulations with two cylinders were carried out in 2D. The results are shown in Table 13 and Fig. 4.

**Table 13** The averaged drag coefficient of the cylinders at different *T/D* ratios (turbulence model: **SAS SST**, $Re$ = 55000). Here $C_D$ was determined as the sum of the time-averaged drag coefficients of the cylinders.

| T/D [-] | $C_D$ |
|---|---|
| 5 | 2.3455 |
| 4 | 2.4470 |
| 3 | 2.5259 |
| 2 | 2.7703 |
| 1.75 | 2.7003 |
| 1.5 | 2.4656 |
| 1.4 | 2.3460 |
| 1.3 | 2.4845 |
| 1.2 | 3.0349 |
| 1.1 | 3.2908 |

**Table 14** The averaged drag coefficient of the cylinders at different *T/D* ratios turbulence model: **SAS SST**, $Re$ = 33610). Here $C_D$ was determined as the sum of the time-averaged drag coefficients of the cylinders.

| T/D [-] | $C_D$ |
|---|---|
| 13 | 2.6816 |
| 11 | 2.6858 |
| 9 | 2.6924 |
| 7 | 2.7216 |
| 5 | 2.6946 |
| 3 | 2.8608 |
| 2 | 3.0258 |
| 1.8 | 3.0068 |
| 1.67 | 2.8644 |
| 1.6 | 2.8164 |
| 1.5 | 2.6626 |
| 1.4 | 2.5140 |
| 1.33 | 2.5882 |
| 1.3 | 2.6468 |
| 1.2 | 3.2040 |
| 1.1 | 3.5054 |
| 1 | 4.3160 |

In Figure 4 the shape of the curve with crosses is quite dissimilar to the curve with squares that belongs to the simple SST model. One can also notice the qualitative resemblance between the SAS SST and the experimental results (curve with crosses and curve with diamonds, respectively) and only a minor difference between the drag coefficients at $T/D$ = 5 and 3. The drag coefficient has a local maximum near $T/D$ = 2 and a local minimum at $T/D$ = 1.4 and increases rapidly when $T/D$ is further decreased. The quantitative difference between the experimental data and our results in the regime where $T/D$ was less than 2 could be explained by the two-dimensional model that was used. In order to prove this, a 3 dimensional model with the same aspect and blockage ratio as Mahbub Alam et al. [13] mentioned was used to simulate the flow around a finite length cylinder in crossflow. The results of this run are shown in Table 15.

**Table 15** The results of the simulations with one cylinder at $Re$ = 33610 and 55000.

| $Re$ [-] | Turbulence model | $C_D$ [-] | Rel.diff [%] |
|---|---|---|---|
| 55000 | Measurement [13] | 1.12 | - |
| | SST (2D) | 0.9492 | -15.25 |
| | SAS SST (2D) | 1.1622 | 3.77 |
| | SST (3D) | 1.1635 | 3.88 |
| | SAS SST (3D) | 1.2019 | 7.31 |
| 33610 | Measurements | 1.2 | - |
| | SST | 0.9492 | 11.3 |
| | SAS SST | 1.1622 | -3.04 |

Table 15 shows that the relative difference of the corrected drag coefficient of the 3D simulation was high (roughly 7.3 %). Taking into account that only cross sectional information was available about the wind-tunnel and the streamwise position of the cylinder from the inlet was undetermined (according to Mahbub Alam et al. [13]) this difference in the drag coefficients is acceptable. Table 15 also suggests that the SAS SST model is more consistent. The difference between the 2D and the 3D results is significantly smaller for the SAS SST model compared to the simple SST model. Note that the drag coefficient at the lower *Re* is closer to the experimental data (1.2) for the SAS SST model (1.1622) than for the SST (0.9492). Based upon the results presented in Table 15 and in Fig. 4 the SAS SST model was chosen for the further simulations. Although the SAS model is in principle designed for 3D problems thus it might be meaningless to use in 2D, our results showed that in practical terms the usage of the SAS SST model is justifiable and provides better results than the SST model.

### 3.2 Two-cylinder arrangements at the original Reynolds number

After the choice between the turbulence models, the SAS SST model was applied to the original Reynolds number (33610, free stream velocity: 2 m/s). In order to have a better understanding on how the cylinders interact with each other, at what distance they start to have an effect on each other and what kind of influence this has on the flow field, a wider $T/D$ range was examined. From $T/D = 13$ to $T/D = 2$ seven, when $T/D$ was below 2, ten different distances were investigated. The results are shown in Table 17 and Fig. 4. The shape of the green curve in Fig. 4 is again similar to both the experimental results and the curve at $Re = 55000$. Figure 5 shows the complete range of distances ($T/D = 1..13$) investigated for $Re = 33610$. The results of the simulations with two cylinders are summarised in Table 17.

**Table 16** The averaged drag coefficient of the cylinders with the different block structures. $\Delta_{rel}$ is the relative difference between the drag coefficients in %.

| O-grid | Number of elements | $C_D$ | $\Delta_{rel}$ [%] |
|---|---|---|---|
| Simple | 47865 | 1.2648 | - |
| Double | 37232 | 1.2570 | 0.615 |

An additional, very small $T/D$ ratio was also simulated. The idea behind this originates from Lorente et al. [4]. This study concluded that the maximum drag appears at the distance of twice the boundary layer thickness around the cylinders. We estimated the boundary layer thickness from the one-cylinder results and then applied this at a two-cylinder arrangement ($T/D = 1.0013$). The result of this simulation is shown in Fig. 4 with an 'X'.

**Table 17** Time-averaged drag coefficient for two cylinders with different $T/D$ ratios. $\Delta_{rel}$ is the relative difference (in %) between the averaged drag coefficients and the $C_D$ of a single cylinder. Figure 4 shows the double of $C_D$ (2 times the values in the second column) versus $T/D$ . This was necessary for the comparison of the results.

| T/D | $C_D$ | $\Delta_{rel}$ [%] |
|---|---|---|
| Single Cylinder | 1.3350 | - |
| 13 | 1.3408 | 0.43 |
| 11 | 1.3429 | 0.59 |
| 9 | 1.3462 | 0.84 |
| 7 | 1.3608 | 1.93 |
| 5 | 1.3473 | 0.92 |
| 3 | 1.4304 | 7.15 |
| 2 | 1.5129 | 13.33 |
| 1.8 | 1.5034 | 12.61 |
| 1.67 | 1.4322 | 7.28 |
| 1.6 | 1.4082 | 5.48 |
| 1.5 | 1.3313 | 0.28 |
| 1.4 | 1.2570 | 5.84 |
| 1.33 | 1.2941 | 3.06 |
| 1.3 | 1.3234 | 0.87 |
| 1.2 | 1.6020 | 20.00 |
| 1.1 | 1.7527 | 31.29 |
| 1 | 2.1580 | 61.65 |

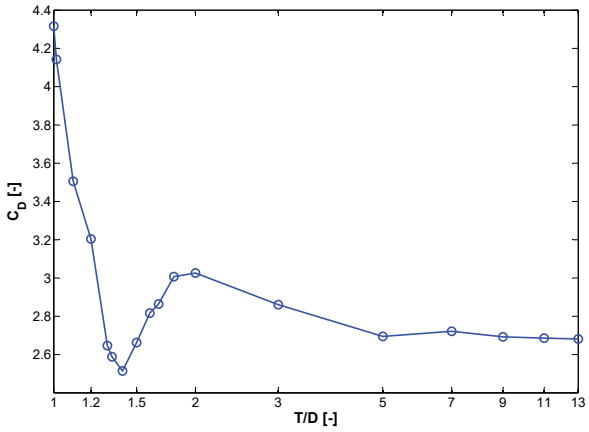


**Fig. 5** Time-averaged drag coefficients versus $T/D$. Here $C_D$ was determined according to Eq. (3).

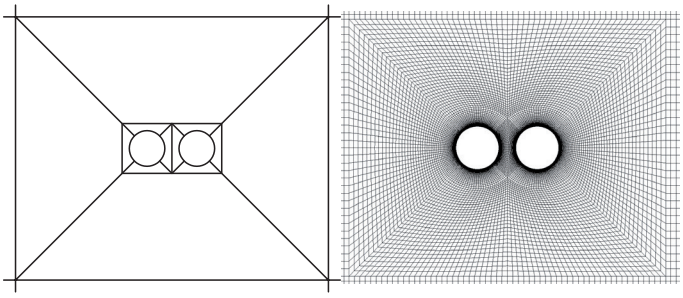

**Fig. 6** The block structure (a) and the mesh (b) around the cylinder at $T/D = 1.4$.

When the two cylinders touched each other ($T/D$ = 1) the geometry of the cylinders was amended to simplify the building of the mesh (Fig. 7).

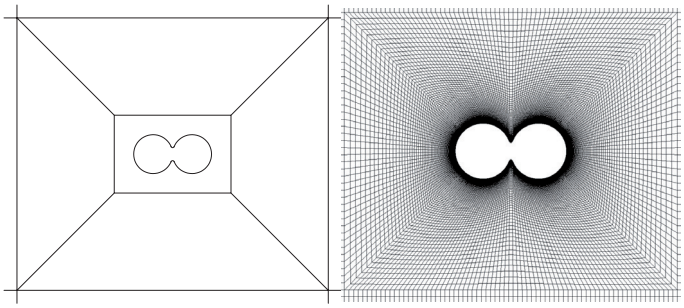

**Fig. 7** The block structure (a) and the mesh (b) around the cylinder at $T/D$ = 1.

Figure 5 shows that when the cylinders are far from each other ($T/D$ = 5..13), the drag coefficient remains almost constant, and is close to the value obtained for the single cylinder (see Fig. 9). From $T/D$ = 5..2 the drag coefficients increase. At $T/D$ = 2 a local maximum of $C_D$ can be observed. When the cylinders are even closer ($T/D$ < 2), the drag coefficients decrease until $T/D$ = 1.4 and then increase apace. Figure 4 suggests that even a very small gap (twice the thickness of the boundary layer around the cylinders, $T/D$ = 1.0013) decreases the drag on the cylinders and the maximum of $C_D$ is at $T/D$ = 1 when the cylinders touch each other.

Animations of the velocity contours were prepared to study the effect of $T/D$ on the fluid flow. When $T/D$ is 13 the two cylinders have no impact on each other, there is no phase relationship in the vortex sheddings from the two cylinders; the cylinders behave like two independent cylinders (Fig. 8).

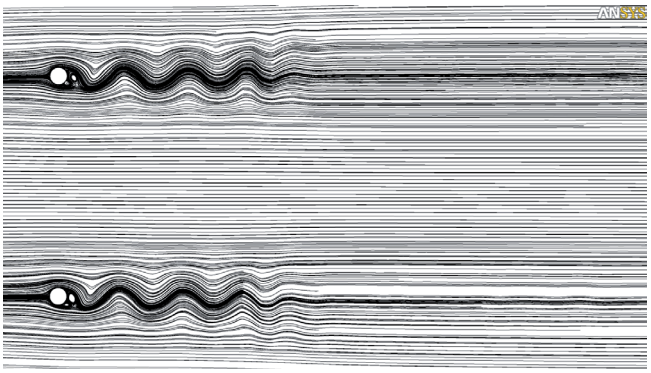

**Fig. 8** Streamlines at $T/D$ = 13

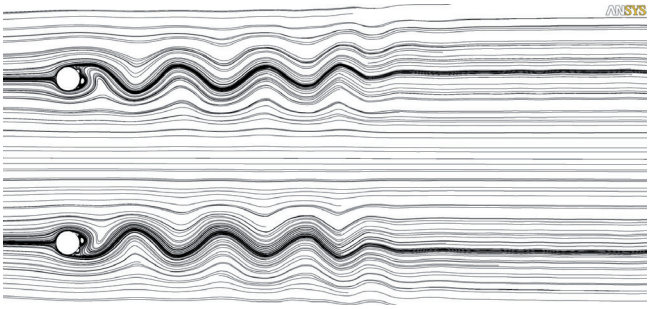

**Fig. 9** Streamlines at $T/D$ = 7

The consistently identical phase is probably due to numerical reasons. At $T/D$ = 11 a small, at $T/D$ = 9 a larger phase difference in the vortex sheddings is observed. When $T/D$ was 7 the phase difference of vortex sheddings increased further and the flow became symmetrical (Fig. 9).

The videos between $T/D$ = 7..2 displayed a very similar picture; the flow remained symmetrical. At $T/D$ = 1.8 for about 1 $s$ (2000 time steps) the flow was symmetrical, then it turned and continued to be asymmetrical until the end of the simulation.

When $T/D$ was 1.67 and 1.6 the duration of the symmetrical flow configuration at the beginning of the simulations decreased. At $T/D$ = 1.5 this symmetrical part was very short, the flow became asymmetrical and chaotic very early. Larger vortices were formed behind one cylinder for approximately 0.6 s (roughly 1200 time steps), shown in Fig. 10. The location of this large vortex changed randomly between the cylinders.

This resulted in an increase of the drag coefficient because the depression caused by the larger vortices was greater. The difference between the time-averaged drag coefficients of the individual cylinders was significant compared to larger $T/D$ ratios. A similar phenomenon was noticed when $T/D$ was 1.4, 1.33 and 1.3. Interestingly, the difference between the two time-averaged $C_D$-s had a maximum at $T/D$ = 1.33. When the distance between the cylinders was smaller ($T/D$ = 1.2 and 1.1) this difference became negligible, just like at large $T/D$ -s but larger vortices were also formed behind the cylinders only for shorter periods of times which resulted almost identical time-averaged $C_D$-s for the cylinders. At $T/D$ = 1 the two cylinder behaved like one single bluff body (Fig. 11) and the flow was similar to the single cylinder case.

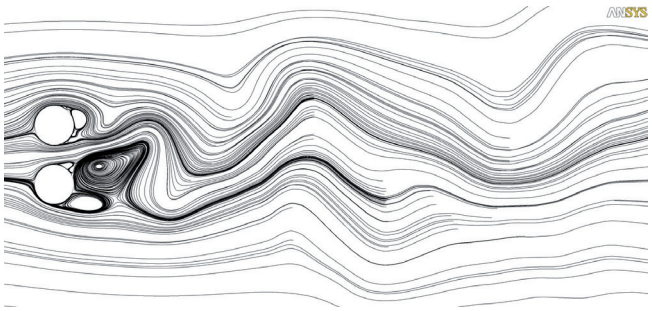

**Fig. 10** Streamlines at $T/D$ = 1.5

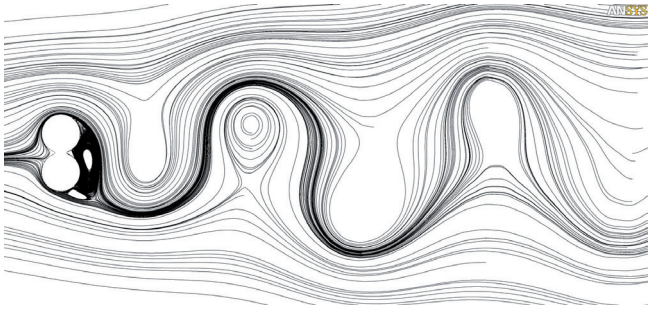

**Fig. 11** Streamlines at $T/D$ = 1

Wang and Zhou [6] investigated the flow behind two cylinders in side-by-side arrangements. According to their results, three regimes can be distinguished considering the flow behind the cylinders. When $T/D$ was smaller than 1.2, the two cylinders behaved like one bluff body and only a single vortex street could be observed. Between $T/D$ = 1.2 and 2, the flow configuration was asymmetrical and the previously mentioned ubiquitous flow pattern appeared. Finally, when $T/D$ was above 2 the flow became symmetrical. Sumner et al. [5] also observed these regimes, the only difference is that the asymetrical one was between $T/D$ = 2.2 and 1.2.

The power spectra of the time-dependent drag coefficients were also evaluated. The spectra were nearly the same for one cylinder and two cylinders when $T/D$ = 13..3 with a dominant frequency at around 60 Hz (see Fig. 12a and 12b), and that is the same as the case of the single cylinder (shown in Fig. 12g).

At $T/D$ = 2 the spectrum displayed several higher harmonics of the 60 Hz frequency but the dominant component of the spectrum – with the largest amplitude – was around 30 Hz, indicating a period-doubling bifurcation (see Fig. 12c).

Below $T/D$ = 2, a subharmonic with a frequency approximately 15 Hz also appears with its higher harmonics (shown in Fig. 12e), as a precursor of a second period doubling.

For $2 > T/D > 1.2$, the spectrum became noisier indicating chaotic behaviour but at $T/D$ = 1.2 and 1.1 it cleared up and some dominant frequencies could be observed which bear no relation to the previously dominant frequencies (Fig. 12e).

At $T/D$ = 1 the signal became periodic again but the frequency of the oscillation shifted to a different value from all previous cases to roughly 23 Hz, as shown in Fig. 12f.

## 4 Four-cylinder arrangements

Having evaluated the results of the two-cylinder arrangements, four-cylinder arrangements were investigated. The same equidistant $T/D$ ratios as before – from 13 to 1 were studied with four cylinders. The size of the computational domain was modified according to the actual $T/D$ ratio to provide enough space on the side of the cylinders. Similarly to the two-cylinder arrangements, the block structure of the mesh was different around the cylinders when $T/D$ was smaller than 1.5 and the geometry was simplified when $T/D$ was 1. The results of the simulations are presented in Table 18.

In Table 18 it can be seen that the time-averaged drag coefficients of the four cylinders are usually larger than those belonging to the two cylinder arrangements. This difference is almost negligible when $T/D > 1.8$ and then it increases rapidly but non monotonically, and has a maximum at $T/D$ = 1.

Between $T/D$ = 13 and 5 the time-averaged drag coefficient is nearly constant. When $1.6 < T/D < 5$, the drag coefficients increase slightly; from $T/D$ = 1.6 to 1.33 the drag coefficients decreased and had a minimum at $T/D$ = 1.33. When $T/D$ was smaller than 1.33 the drag coefficients increased apace and had a maximum at $T/D$ = 1 (similarly to the two cylinder arrangements), see Fig. 13.

**Table 18** Time-averaged drag coefficient for two ($C_{D,2}$) and four ($C_{D,4}$) cylinders arrangements versus $T/D$. $\Delta_{rel}$ is the relative difference (in %) between the time-averaged drag coefficients, whereby the two-cylinder results were used as a basis.

| $T/D$ | $C_{D,4}$ | $C_{D,2}$ | $\Delta_{rel}$ [%] |
|---|---|---|---|
| 13 | 1.350 | 1.341 | 0.67 |
| 11 | 1.353 | 1.343 | 0.78 |
| 9 | 1.358 | 1.346 | 0.90 |
| 7 | 1.377 | 1.361 | 1.17 |
| 5 | 1.383 | 1.347 | 2.60 |
| 3 | 1.521 | 1.430 | 5.94 |
| 2 | 1.503 | 1.513 | 0.64 |
| 1.8 | 1.500 | 1.503 | 0.25 |
| 1.67 | 1.526 | 1.432 | 6.16 |
| 1.6 | 1.556 | 1.408 | 9.47 |
| 1.5 | 1.524 | 1.331 | 12.66 |
| 1.4 | 1.440 | 1.257 | 12.73 |
| 1.33 | 1.429 | 1.294 | 9.45 |
| 1.3 | 1.482 | 1.323 | 10.69 |
| 1.2 | 1.807 | 1.602 | 11.32 |
| 1.1 | 1.983 | 1.752 | 11.63 |
| 1 | 2.773 | 2.158 | 22.18 |

Figure 14 shows the time-averaged drag coefficients of the individual cylinders (in four cylinder arrangements).

We also looked at the drag coefficients of the individual cylinders. When $T/D > 1.6$ the drag coefficient is almost the same; from $T/D$ = 1.6 to 1 the difference between the time-averaged drag coefficients gets larger and larger and has a maximum at $T/D$ = 1.1. The time-averaged drag coefficients of the two inner cylinders were usually larger than the drag coefficients of the two outer ones, because most of the time larger wakes were formed behind the inner cylinders. For the two-cylinder arrangements, this difference $\Delta_{C_D}$) was much smaller and the relation between $\Delta_{C_D}$ and $T/D$ was not as clear as in the four cylinder arrangements.

Videos of the velocity contours were also evaluated. These showed that at $T/D$ = 13, 11 and 9 the flow was very alike: the vortex sheddings from the cylinders were independent of each other, the cylinders behaved like individual bluff bodies (see Fig. 16). From $T/D$ = 7 to 3 the flow was nearly symmetrical (see Fig. 17 and Fig. 18), the vortex shedding from the outer cylinders was the same as for larger $T/D$ ratios while from the inner ones they were almost in the opposite phase. When $T/D$ was 2 and 1.8 the ow was asymmetrical (see Fig. 19) but the nature of the vortex sheddings were same as for $3 < T/D < 7$. From $T/D$ = 1.67 to 1.2 the flow was asymmetrical and chaotic (see Fig. 20),

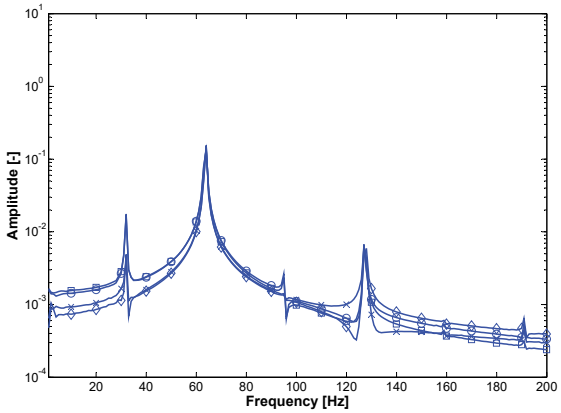


(a) $T / D = 13$

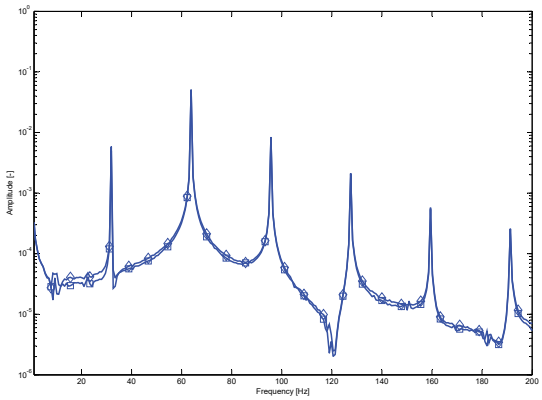


(b) $T / D = 3$

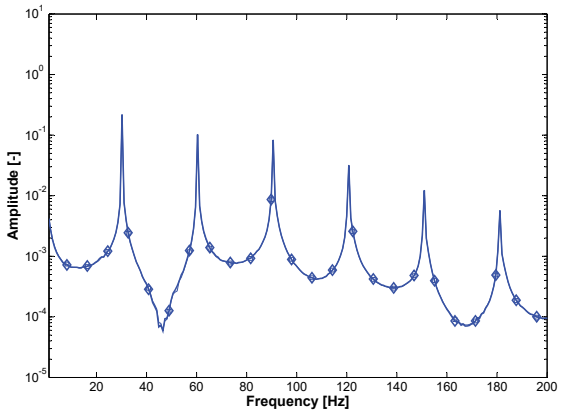


(c) $T / D = 2$

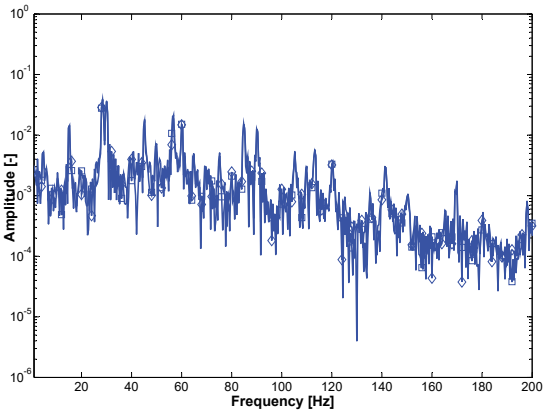


(d) $T / D = 1.8$

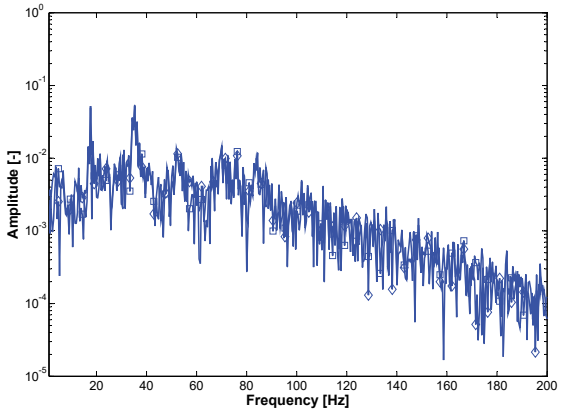


(e) $T / D = 1.2$

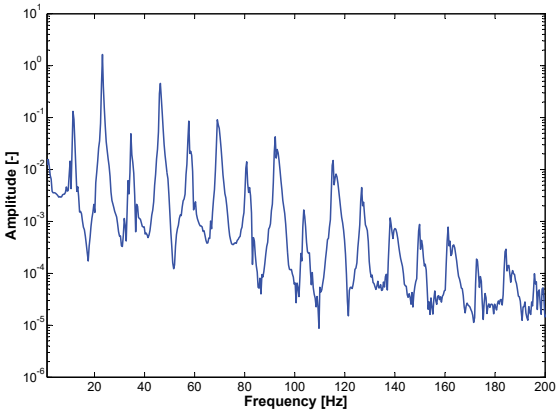


(f) $T / D = 1$

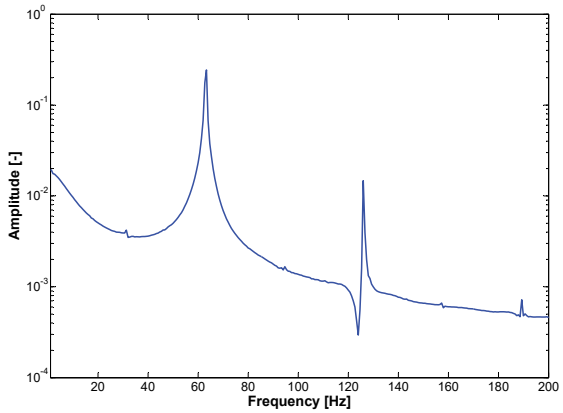


(g) Single cylinder

**Fig. 12** The power spectrum of the drag coefficients of two cylinders at different $T / D$ ratios.

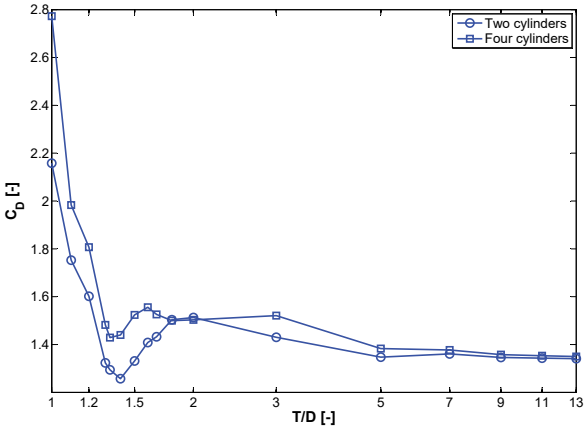


**Fig. 13** Time-avaraged drag coefficients versus $T / D$.

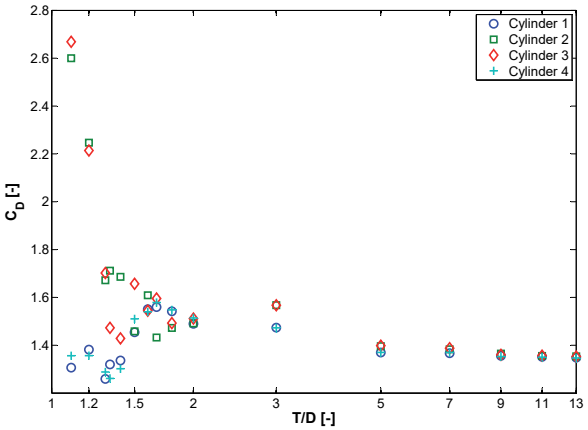


**Fig. 14** Time-avaraged drag coefficients of the four individual cylinders.

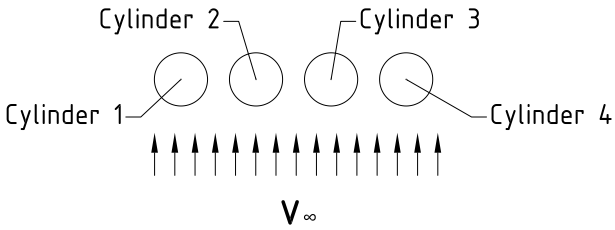


**Fig. 15** The order of the cylinders during four-cylinder arrangements.

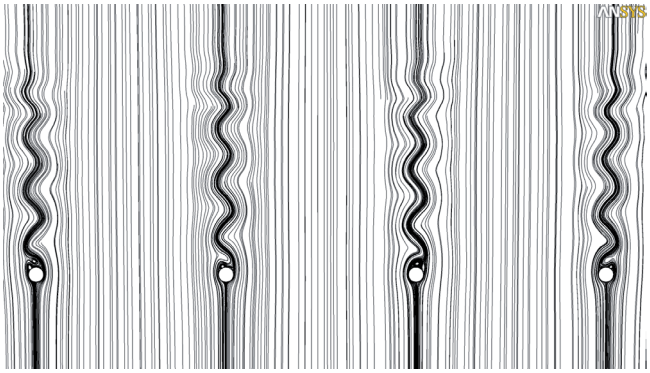

**Fig. 16** Streamlines at $T/D = 13$

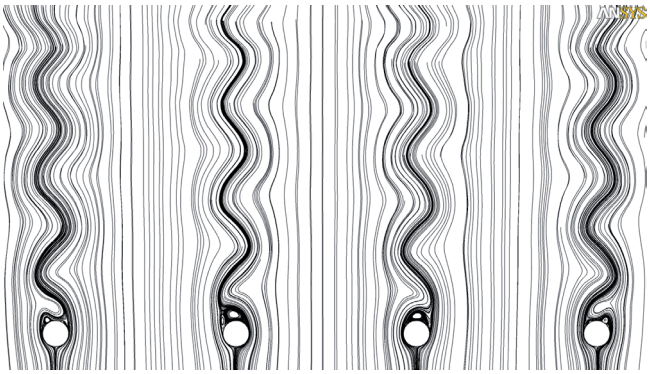

**Fig. 17** Streamlines at $T/D = 7$

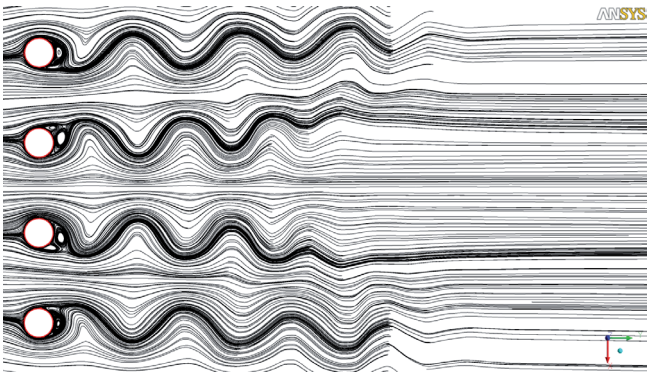

**Fig. 18** Streamlines at $T/D = 3$

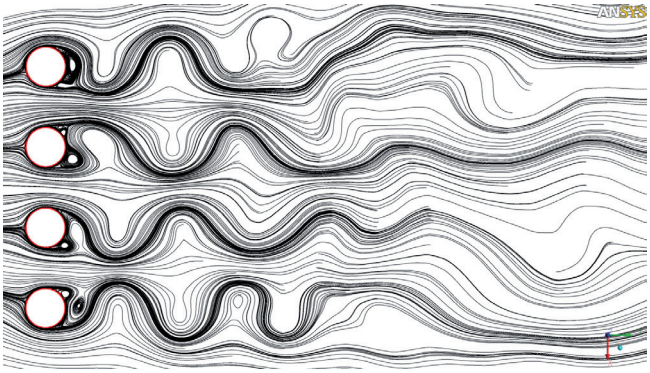

**Fig. 19** Streamlines at $T/D = 2$

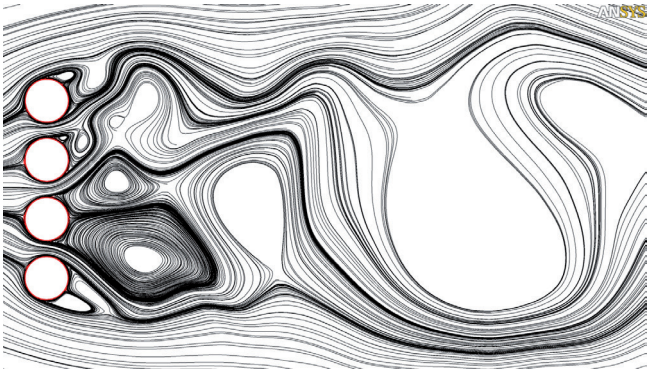

**Fig. 20** Streamlines at $T/D = 1.33$

the time-averaged drag coefficients were different for the individual cylinders: generally, behind one of the two inner cylinders a larger wake was formed for longer periods of time which resulted in an increase of the time-averaged drag coefficient. When T/D was 1.1 and 1 the four cylinders behaved like a single bluff body in terms of vortex shedding (shown in Fig. 21).

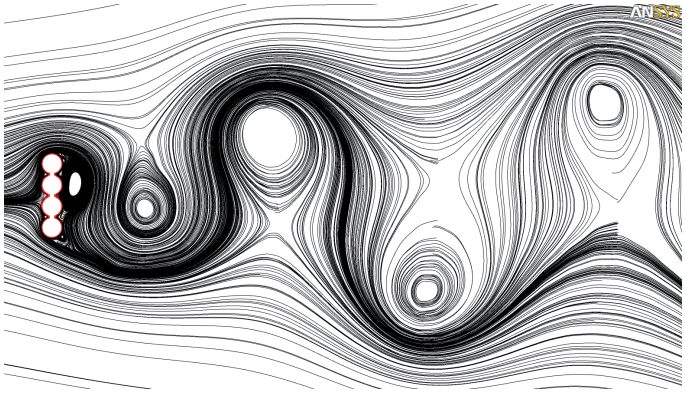

**Fig. 21** Streamlines at $T/D = 1$

The power spectra of the drag coefficients were studied as well. From $T/D = 13$ to 3, these spectra were very similar, with a dominant frequency at around 65 Hz (shown in Fig. 22a and 22b). The only difference was the amplitude of the higher and subharmonics: as $T/D$ decreased, the amplitudes of these harmonics increased. For $T/D = 2$ and 1.8 the spectra became noisier but a dominant frequency for the two outer cylinders (at around 30 Hz) and the inner cylinders (at around 60 Hz) could be distinguished (Fig. 22c). When $T/D$ was smaller than 1.8 the spectra were very noisy and no dominant frequencies could be distinguished (see Fig. 22d). At $T/D = 1$ the spectrum was less noisy and the dominant frequency with the largest amplitude was at roughly 10 Hz (shown in Fig. 22e), which again bears no relation to the dominant frequencies of the flows at large $T/D$ ratios.

Sumner et al. [5] studied not just two but three cylinders in a crossflow. They distinguished four regimes by $T/D$. When $T/D$ was larger than 2.2 the vortex shedding from the different cylinders were unbiased and the cylinder had almost no effect on each other in terms of vortex shedding. From $1.35 < T/D < 2.2$ the flow was symmetrical and a larger wake was formed behind the middle cylinder. When $T/D$ was between 1.35 and 1.125 the larger wake was formed behind one of the outer cylinders and thus the flow became asymmetrical. At smaller $T/D$ values the three cylinders behave like one single bluff body.

The results and flow patterns of our four-cylinder arrangements – as described before – show quite good resemblance to those of the previously mentioned three-cylinder arrangements. When $2 < T/D < 13$ the vortex sheddings from the four cylinders were independent. Between $T/D = 2$ and 1.2 the flow was asymmetrical and larger wakes were formed behind the inner two cylinders. At $T/D = 1.1$ and 1 the vortex sheddings were just like for three cylinders.

## 5 Discussion

Contrary to the expectations we found both for the two- and the four-cylinder arrangements that the maximum of the time-averaged drag coefficient is at zero gap. The expectation, supported by several studies in the literature, was that there is a small gap providing the maximum of the drag coefficient. The physical idea behind this expectation was that a small gap does not influence the form drag compared to the zero gap case, whereas it provides an additional frictional drag from the flow between the fingers. At the end, this idea proved to be erroneous for the following reason. With the introduction of any gap, the form drag decreased radically because the pressure difference between the two sides of a 'plate' was reduced by the communication through the gaps. At the same time the frictional drag did not compensate for this because it had a value two orders of magnitude smaller than the form drag and its increase was negligible compared to the decrease of the form drag.

Another interesting question is, when we can consider the cylinders to behave independently of each other. On the one hand, one can argue that the cylinders are independent in the region where the drag coefficient is independent of T/D and its value is similar to that of a single cylinder. On the other hand, even if the cylinders are far away, they have a fixed phase relationship which clearly indicates that they influence each other and in this sense do not behave independently. However, it may be just a numerical effect.

We can notice that in the "non-independent" region, the two-cylinder arrangement leads to a higher average drag coefficient than the single cylinder, and the four-cylinder arrangement to an even higher one. This tells us that simply the presence of further cylinders makes the individual wakes interfere with each other, thereby increasing the drag.

## 6 Conclusion

Our goal with this study was to investigate the effect of the finger spacing in human swimming. Two-dimensional **CFD** simulations with two and four cylinders were carried out to resolve this problem. Because of this simplified model of the fingers,the impact of the thumb could not be examined. First, only one cylinder was investigated thoroughly to find the appropriate computational domain size, mesh size and turbulence model for the two- and four-cylinder arrangements. After this, several $T/D$ ratios were simulated with two and four cylinders. The time-averaged drag coefficients of the cylinders were compared and videos of the velocity contours were evaluated. The flow patterns of our simulations showed good resemblance with the literature. Three different flow configurations could be observed for the two- and the four-cylinder arrangements. When $T/D$ was over 2, the vortex shedding from the cylinders was independent. From $T/D = 1$ to 2, the flow became asymmetrical and larger wakes were formed behind one of the cylinders for longer

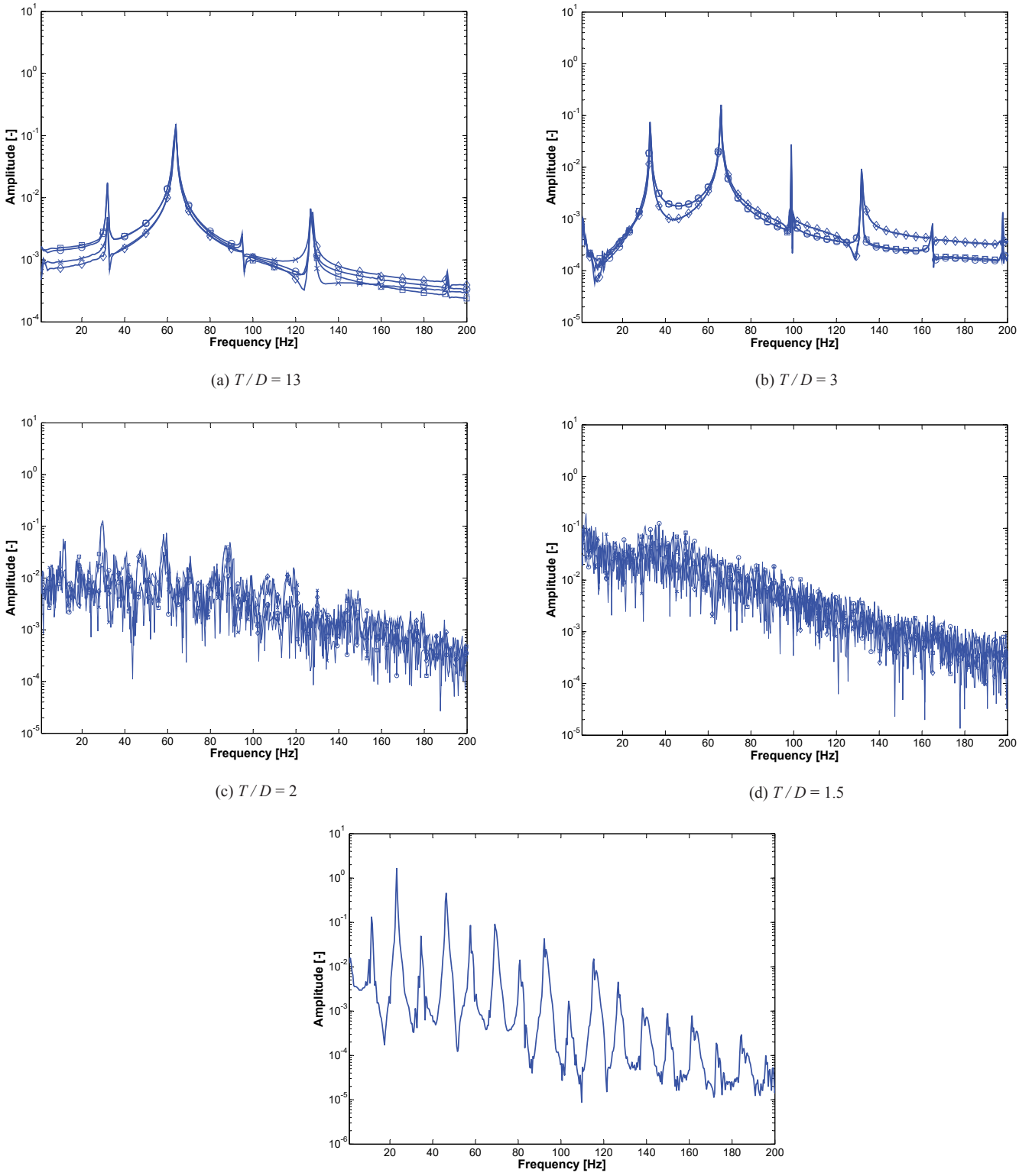


(a) $T/D = 13$

(b) $T/D = 3$

(c) $T/D = 2$

(d) $T/D = 1.5$

(e) $T/D = 1$

**Fig. 22** The power spectra of the drag coefficients at different $T/D$ ratios. Legend: *Lines with circles: Cylinder 1; Lines with squares: Cylinder 2; Lines with diamonds: Cylinder 3; Lines with crosses: Cylinder 4* (for cylinder arrangment, see Fig. 15)

periods of times. When there was no gap between the cylinders ($T/D = 1$), only one vortex street could be distinguished. These three regimes were also mentioned by Sumner et al. [5] and Mahbub Alam et al. [13] in their studies. Signs of period-doubling bifurcations were discovered with the reduction of the $T/D$ ratio.

The optimum finger spacing proved to be different from what other simulations – both 2D and 3D – showed. For both two and four cylinders, the maximum of $C_D$ was at $T/D = 1$, i.e. no gap. This means that – according to this very simple model - a swimmer can produce larger force with his hand if his fingers are closed.

## References


[1] Marinho, D. A., Barbosa, T. M., Reis, V. M., Kjendlie, P. L., Alves, F.B., Vilas-Boas, J. P., Machado L., Silva A. J., Rouboa A. I. "Swimming Propulsion Forces Are Enhanced by a Small Finger Spread." *Journal of Applied Biomechanics*. 26 (1). pp. 87-92. 2010.

[2] Minetti, A. E., Machtsiras, G., Masters, J. C. "The optimum finger spacing in human swimming." *Journal of Biomechanics*. 42 (13). pp. 2188-2190. 2009. DOI: 10.1016/j.jbiomech.2009.06.012

[3] Bilinauskaite, M., Mantha, V. R., Rouboa, A. I., Ziliuskas, P., Silva, A. J. "Computational fluid dynamics study of swimmer's hand velocity, orientation and shape: Contributions to hydrodynamics." *BioMed Research International*. ID 140487. 2013. DOI: 10.1155/2013/140487

[4] Lorente, S., Cetkin, E., Bello-Ochende, T., Meyer, J. P., Bejan, A. "The constructal-law physics of why swimmers must spread their fingers and toes." *Journal of Theoretical Biology*. 308. pp. 141-146. 2012. DOI: 10.1016/j.jtbi.2012.05.033

[5] Sumner, D., Wong, S. S. T., Price, S. J., Paidoussis, M. P. "Fluid behaviour of side-by-side circular cylinder in steady cross-flow." *Journal of Fluids and Structures*. 13 (3). pp. 309-338. 1999. DOI: 10.1006/jfls.1999.0205

[6] Wang, Z. J., Zhou, Y. "Vortex interactions in a two side-by-side cylinder near-wake." *International Journal of Heat and Fluid Flow*. 26 (3). pp. 362-377. 2005. DOI: 10.1016/j.ijheatfluidflow.2004.10.006

[7] Bruschi, G., Tsang, K., Nishioka, T., Wang, R. "Drag coefficient of a cylinder." 2003. URL: http://www.disasterzone.net/projects/docs/mae171a/water_tunnel_experiment.pdf

[8] Tritton, D. J. "*Physical fluid dynamics*." Oxford University Press, Oxford, England, 1988.

[9] Hover, F. S., Tvedt, H., Triantafyllou, M. S., Wang, R. "Vortex-induced vibrations of a cylinder with tripping wires." *Journal of Fluid Mechanics*. 448. pp. 175-195. 2001. DOI: 10.1017/S0022112001005985

[10] Dynnikova, G. Y. "The viscous vortex domains (VVD) method for nonstationary viscous incompressible flow simulation." In: *IV. European Conference on Computational Mechanics*. Palais de Congrés, Paris, France, May 2010.

[11] Benim, A. C., Cagan, M., Nahavandi, A., Pasqualotto, E. "RANS predictions of turbulent flow past a cricular cylinder over the critical regime." In: *Proceedings of the 5th IASME / WSEAS International Conference on Fluid Mechanics and Aerodynamics*, Athens, Greece, August 25-27, 2007. pp. 235-240. 2007.

[12] Techet, A. H. "Vortex induced vibrations." 2005. URL: http://ocw.mit.edu/courses/mechanical-engineering/2-22-design-principles-for-ocean-vehicles-13-42-spring-2005/readings/lec20_viv1.pdf

[13] Mahbub Alam, Md., Moriya, M., Sakamoto, H. "Aerodynamic characteristics of two side-by-side circular cylinders and application of wavelet analysis on the switching phenomenon." *Journal of Fluids and Structures*. 18 (3-4). pp. 325-346. 2003. DOI: 10.1016/j.jfluidstructs.2003.07.005